Theoretical Study of the Mechanism of Carbonyl Insertion Reactions Catalyzed by Nickel Complexes

Fernando Bernardi, Andrea Bottoni,* Marco Nicastro, and Ivan Rossi

Dipartimento di Chimica "G. Ciamician", Università di Bologna, via Selmi 2, 40126 Bologna, Italy

Juan Novoa and Xavier Prat

Department Quimica Fisica, Facultat Quimica, University of Barcelona, Av. Diagonal 647, 08028-Barcelona, Spain

Received October 12, 1999

A theoretical study of the catalyzed carbonylation process on the model system $CH_3-Ni(CO)_2Cl$ reacting with a CO molecule has been carried out using a DFT approach. It has been found that two different reaction channels lead to the carbonylation products (acyl complexes). Along one reaction channel the carbonyl insertion takes place on five-coordinated nickel complexes, while the other reaction channel only involves the formation of four-coordinated complexes. The two reaction pathways require the overcoming of similar energy barriers for the insertion process (the barriers for the rate-determining step are 4.36 and 6.83 kcal mol^{-1} in the two cases, respectively). Even if for the model system considered here one reaction channel is slightly more convenient than the other, the computational results suggest that for the real system the two reaction paths can become highly competitive and their relative importance can change depending on the experimental conditions.

Introduction

Carbonylation reactions catalyzed by transition-metal complexes represent an important synthetic tool widely used in both industry and academic laboratories to obtain acid derivatives, aldehydes, and ketones.[1] The "oxo" process, for instance, also often referred to as "hydroformylation", is used on an industrial scale to convert olefins and synthesis gas into aldehydes by means of cobalt and rhodium complexes as catalysts. The Monsanto reaction is another example of a commercially very important process which is used worldwide to form acetic acid from methanol in an extremely selective and fast way. Because of their relevance a great deal of experimental work[1] has been carried out on carbonylation reactions. All these studies indicate as the essential step the insertion of a carbon monoxide molecule (CO) into a metal−carbon bond.

A number of theoretical studies on carbonyl insertion using different model systems has also appeared in the literature during the last two decades.[2] Many of these papers describe the insertion of a carbonyl into a metal−carbon bond and point out, in agreement with the experimental evidence, that in these processes an alkyl group actually migrates from the metal to the carbonyl ligand; for this reason the reaction is also called migratory insertion. However, while the processes catalyzed by Mn, Pd, Pt, and Rh have been described in detail, only a few papers have considered the reactions involving the nickel−carbon bond. Thus, there is still a general lack of information on the details of the nickel-catalyzed insertion step even though quite recently, in a theoretical paper on the related Reppe carbonylation, the insertion of CO into the $Ni-CH=CH_2$ bond has been investigated at the DFT level using both static and dynamic approaches.[2m] It has been found that the reaction, which is exothermic by about 4 kcal mol^{-1}, proceeds through the formation of four-coordinated intermediate complexes.

In the present paper we focus our attention on carbonylation processes catalyzed by nickel tetracarbonyl, $Ni(CO)_4$, which are used to convert simple olefins into saturated carboxylic acids and esters. The accepted mechanism for these reactions assumes that $Ni(CO)_4$ dissociates into nickel tricarbonyl, $Ni(CO)_3$, and carbon monoxide. $Ni(CO)_3$ is a coordinatively unsaturated species which should represent the real active catalyst.[1b] The reaction of $Ni(CO)_3$ with hydrogen chloride added to the reaction medium (step a) gives the

(1) (a) Bird, C. W. *Chem. Rev.* **1962**, *62*, 283. (b) Day, J. P.; Basolo, F.; Pearson, R. G. *J. Am. Chem. Soc.* **1968**, *90*, 6927. (c) Cassar, L.; Chiusoli, G. P.; Guerrieri, F. *Synthesis* **1973**, 509. (d) Wojcicki, A. *Adv. Organomet. Chem.* **1973**, *11*, 88. (e) Garrou, P. E.; Heck, R. F. *J. Am. Chem. Soc.* **1976**, *98*, 4115. (f) Calderazzo, F. *Angew. Chem., Int. Ed. Engl.* **1977**, *16*, 299. (g) Kuhlmann, E. J.; Alexander, J. J. *Coord. Chem. Rev.* **1980**, *33*, 195. (h) Anderson, G. K.; Cross, R. J. *Acc. Chem. Res.* **1984**, *17*, 67.

(2) (a) Berke, H.; Hoffmann, R. *J. Am. Chem. Soc.* **1978**, *100*, 7225. (b) Saddei, D.; Freund, H. J.; Hohlneicher, G. *J. Organomet. Chem.* **1980**, *186*, 63. (c) Sakaki, S.; Kitaura, K.; Morokuma, K.; Ohkubo, K. *J. Am. Chem. Soc.* **1983**, *105*, 2280. (d) Anderson, G. K.; Cross, R. J. *Acc. Chem. Res.* **1984**, *17*, 67. (e) Ziegler, T.; Versluis, L.; Tschinke, V. *J. Am. Chem. Soc.* **1986**, *108*, 612. (f) Rappé, A. K. *J. Am. Chem. Soc.* **1987**, *109*, 5605. (g) Dedieu, A.; Sakaki, S.; Strich, A.; Siegbahn, P. E. M. *Chem. Phys. Lett.* **1987**, *133*, 317. (h) Axe, F. U.; Marynick, D. S. *Chem. Phys. Lett.* **1987**, 141, 455. (i) Axe, F. U.; Marynick, D. S. *J. Am. Chem. Soc.* **1988**, *110*, 3728. (j) McKee, M. L.; Dai, C. H.; Worley, S. D. *J. Phys. Chem.* **1988**, *92*, 1056. (k) Koga, N.; Morokuma, K. *New J. Chem.* **1991**, *15*, 749. (l) Matsubara, T.; Koga, N.; Ding, Y.; Musaev, D. G.; Morokuma, K. *Organometallics* **1997**, *16*, 1065. (m) De Angelis, F.; Re, N.; Sgamellotti, A.; Selloni, A.; Weber, J.; Floriani, C. *Chem. Phys. Lett.* **1998**, *291*, 57.

10.1021/om990808w CCC: $19.00
Publication on Web 04/28/2000

Scheme 1

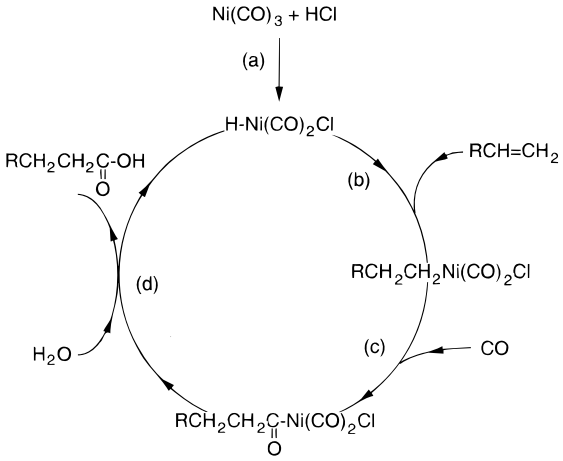

nickel hydride $HNi(CO)_2Cl$, which attacks the olefin substrate $RCH{=}CH_2$ to form the alkyl complex RCH_2-$CH_2Ni(CO)_2Cl$ by insertion into the Ni−H bond (step b). In a subsequent step (step c) carbon monoxide inserts into the Ni−C bond to give the acyl complex RCH_2-$CH_2(CO)Ni(CO)_2Cl$ (the mechanism is reported in Scheme 1 as a catalytic cycle). However, many aspects of this mechanism are still obscure. In particular, it is not evident if intermediate complexes are involved in the insertion step and the nature (structure and coordination of the metal) of these intermediate species has not been clarified yet. While a number of studies point out that no intermediate complexes can be isolated, Garrou and Heck in a thorough investigation of the mechanism of carbonylation of organoplatinum, organopalladium, and organonickel complexes,[1e] $M(R)(Cl)(PR'_3)_2$ (M = Pt, Pd, Ni), carried out in tetrachloroethane at 1 atm of CO, have interpreted their kinetic data in terms of formation of both four-coordinated and five-coordinated intermediates. They have suggested that the carbonyl insertion can take place on both intermediates, depending on the reaction conditions.

To shed light on these mechanistic aspects, we have carried out at the DFT level[3] a detailed study of the potential energy surface associated with the CO insertion step (step c in Scheme 1). Our model system is formed by the methylnickel complex $CH_3Ni(CO)_2Cl$, which can interact with an additional CO molecule. The reaction pattern that we have examined is summarized in Scheme 2. In this scheme we have considered two possible reaction paths: path a (addition−insertion path) and path b (insertion−addition path). In the former case a CO molecule interacts with the coordinatively unsaturated four-coordinated complex **1** to give the five-coordinated saturated intermediate **2** which then leads to the final acyl product **3**, when one of the CO ligands inserts into the Ni−C bond. In the latter case the four-coordinated complex **1** first recombines to form the highly unsaturated acyl complex **4**, which can easily bind an additional CO molecule to generate the product **3**.

Computational Methods

All the DFT computations reported here have been performed with the Gaussian 98[4] series of programs using Becke's hybrid three-parameter exchange functional.[5] Several critical points of the potential surface have also been recomputed with the pure BP86 functional.[6]

The 6-31G* basis set[7] has been used for carbon, hydrogen, oxygen, and chlorine atoms, while the nickel atom has been described by the 6-311G* basis provided by Gaussian 98. This basis corresponds to the Watchers−Hay basis,[8] using the scaling factors of Raghavachari and Trucks.[9] In all cases the geometries of the various critical points have been fully optimized with the gradient method available in Gaussian 98 and the nature of each critical point has been characterized by computing the harmonic vibrational frequencies.

To check the reliability of our computational approach, we have used the B3LYP functional to study the decomposition reaction

$$Ni(CO)_4 \rightarrow Ni(CO)_3 + CO \qquad (1)$$

which provides the catalytically active form. We have found that this process is endothermic by 22.01 kcal mol^{-1}. This value is consistent with the experimental results of Day, Pearson, and Basolo,[10] who obtained for this endothermic reaction an activation enthalpy of 22.1 kcal mol^{-1}. It also agrees fairly well with a bond dissociation energy (Ni−CO) of 23.6 kcal mol^{-1} obtained at the CCSD(T) level.[11]

Scheme 2

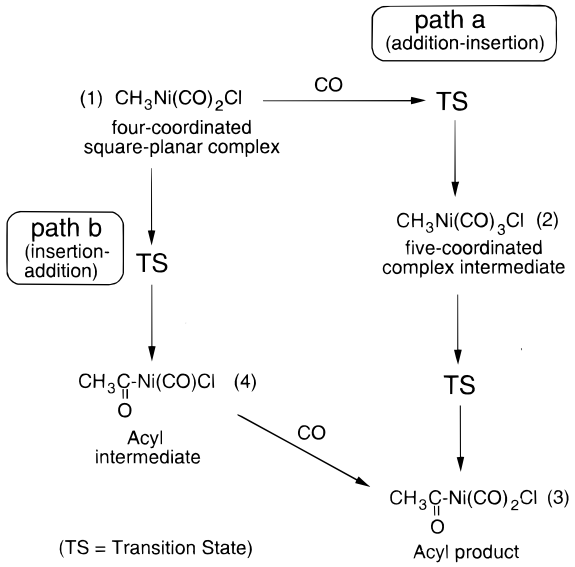

(3) Parr, R. G.; Yang, W. *Density-Functional Theory of Atoms and Molecules*; Oxford University Press: New York, 1989.

(4) Frisch, M. J.; Trucks, G. W.; Schlegel, H. B.; Scuseria, E. G.; Robb, M. A.; Cheeseman, J. R.; Zakrzewski, V. G.; Montgomery, J. A.; Stratmann, R. E.; Burant, J. C.; Dapprich, S.; Millam, J. M.; Daniels, A. D.; Kudin, K. N.; Strain, M. C.; Farkas, O.; Tomasi, J.; Barone, V.; Cossi, M.; Cammi, R.; Mennucci, B.; Pomelli, C.; Adamo, C.; Clifford, S.; Ochterski, J.; Petersson, G. A.; Cui, Q.; Morokuma, K.; Malik, D. K.; Rabuck, A. D.; Raghavachari, K.; Foresman, J. B.; Cioslowski, J.; Ortiz, J. V.; Stefanov, B. B.; Liu, G.; Liashenko, A.; Piskorz, P.; Kamaromi, I.; Gomperts, R.; Martin, R. L.; Fox, D. J.; Keith, T.; Al-Laham, M. A.; Peng, C. Y.; Nanayakkara, A.; Gonzalez, C.; Challacombe, M.; Gill, P. M. W.; Johnson, B. G.; Chen, W.; Wong, M. W.; Andres, J. L.; Gonzalez, C.; Head-Gordon, M.; Replogle, E. S.; Pople, J. A. Gaussian 98, Revision A.6; Gaussian, Inc., Pittsburgh, PA, 1998.

(5) Becke, A. D. *J. Chem. Phys.* **1993**, *98*, 5648.

(6) Perdew, J. P. *Phys. Rev. B* **1986**, *23*, 5048.

(7) (a) Hehre, W. J.; Ditchfield, R.; Pople, J. A. *J. Chem. Phys.* **1972**, *56*, 2257. (b) Hariharan, P. C.; Pople, J. A. *Theor. Chim. Acta* **1973**, *28*, 213. (c) Binkley, J. S.; Pople, J. A. *J. Chem. Phys.* **1977**, *66*, 879. (d) Francl, M. M.; Pietro, W. J.; Hehre, W. J.; Binkley, J. S.; Gordon, M. S.; Defrees, D. J.; Pople, J. A. *J. Chem. Phys.* **1982**, *77*, 3654.

(8) Wachters, A. J. H. *J. Chem. Phys.* **1970**, *52*, 1033.

(9) Raghavachari, K.; Trucks, G. W. *J. Chem. Phys.* **1989**, *91*, 1062.

(10) Day, J. P.; Pearson, R. G.; Basolo, F. *J. Am. Chem. Soc.* **1968**, *90*, 6933.

(11) Dapprich, S.; Pidun, U.; Ehlers, A. W.; Frenking, G. *Chem. Phys. Lett.* **1995**, *242*, 521.

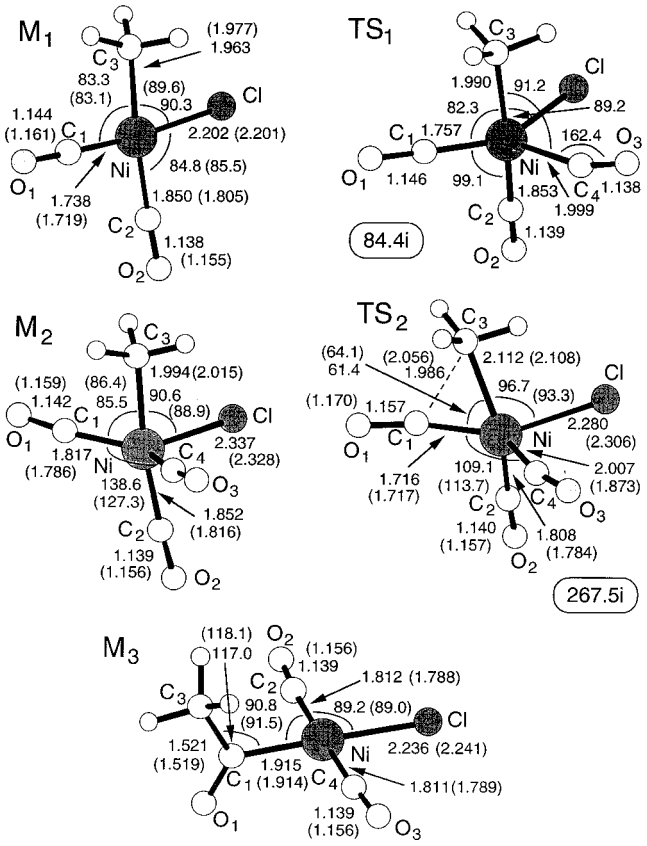

Figure 1. Schematic representation of the molecular structures found on path a for the *cis* four-coordinated complex. Values were obtained with the B3LYP and BP86 (in parentheses) functionals (bond lengths are in angstroms and angles in degrees). The values of the imaginary frequency are reported for the transition structures.

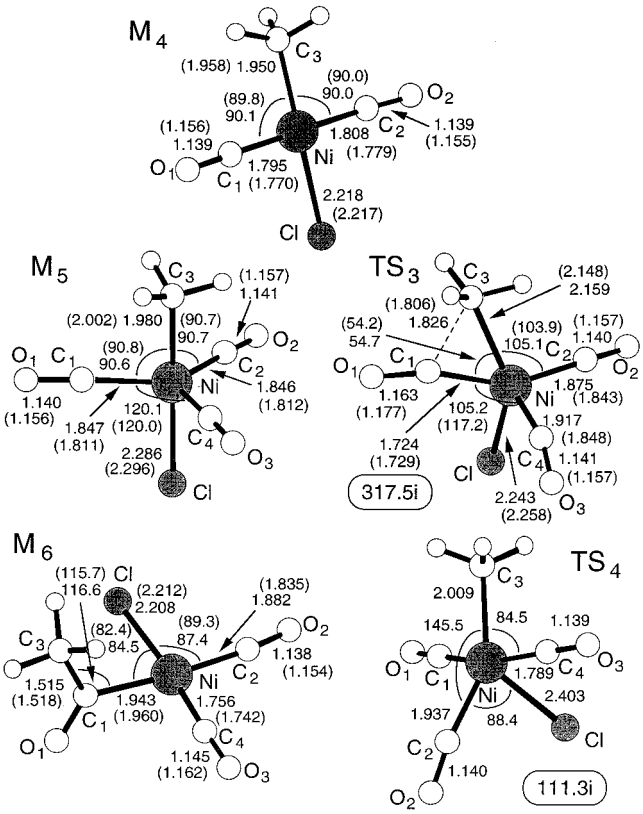

Figure 2. Schematic representation of the molecular structures found on path a for the *trans* four-coordinated complex and Berry transition state (TS_4). Values were obtained with the B3LYP and BP86 (in parentheses) functionals (bond lengths are in angstroms and angles in degrees). The values of the imaginary frequency are reported for the transition structures.

Results and Discussion

We have considered the two possible isomers of the tetracoordinated complex **1**. We call the *cis* isomer the structure where the two CO ligands are adjacent and the *trans* isomer the species where the two CO ligands are opposite. For each isomer we have investigated the two possible reaction paths (path a and path b) reported in Scheme 2. All the results are collected in Figures 1−7.

A. Path a (Addition−Insertion Mechanism). A schematic representation of the molecular structures corresponding to the various critical points is given in Figure 1 (*cis* isomer) and Figure 2 (*trans* isomer). The values of the most relevant geometrical parameters are also reported in the figures, while the corresponding energy values are collected in the diagrams of Figures 3 and 4. We discuss first in detail the results obtained for the reaction path associated with the *cis* isomer M_1 (*cis* path). M_1 corresponds to a tetracoordinated square-planar complex where the nickel−carbonyl bond (Ni−C_2) which is *anti* to the methyl group is significantly longer (1.850 Å) than the nickel−carbonyl bond (Ni−C_1) adjacent to the methyl group (1.738 Å). Complex M_1 can bind an additional CO ligand through the transition state TS_1 leading to the pentacoordinated complex M_2. The new CO ligand approaches the square complex along a direction which is approximately orthogonal to the M_1 molecular plane. A comparison between the transition state TS_1 and the resulting complex M_2 shows that in TS_1 the newly forming nickel−carbon bond (Ni−C_4) is only slightly longer than the final equilibrium value: this bond length changes from 1.999 Å (in TS_1) to 1.817 Å in M_2. As a consequence of the almost complete nickel−carbon bond a significant distortion with respect to planarity has been found in TS_1, the Cl−Ni−C_1 angle being 146.7° (180° in M_1). The five-coordinated complex M_2, which forms after binding the additional CO ligand, is coordinatively saturated and has a C_2 symmetry with the symmetry plane corresponding to the Cl−Ni−C_3 plane. An additional transition state TS_2 leads from the complex M_2 to the final acyl product M_3. In TS_2 the methyl fragment is actually migrating from the metal to the carbon atom, as indicated by the transition vector associated with the imaginary frequency reported in the figure: this vector is dominated by the breaking Ni−C_3 bond and the newly forming C_3−C_1 bond: the breaking bond is 2.112 Å, the forming bond is 1.986 Å, and the angle between these two bonds is 61.4°. A computation of the intrinsic reaction coordinate (IRC), starting from TS_2, shows that this transition state leads directly to the acyl product M_3 without involving additional intermediates. M_3 is a four-coordinated square-planar nickel complex that has a C_2 symmetry and the two CO ligands in *trans* positions. The new C_1−C_3 bond of the acyl group, originated by the insertion−migration process, lies in the molecular symmetry plane.

A similar potential energy surface has been found for the reaction path associated with the *trans* isomer M_4

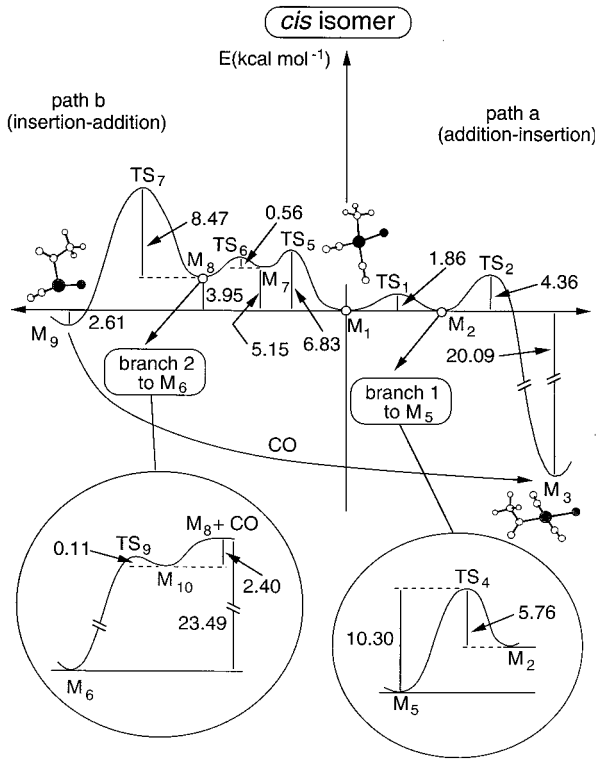

Figure 3. Schematic representation of the energy profiles for the two reaction paths a and b that originate from the *cis* four-coordinate complex M_1. The absolute energies (hartrees) are as follows: *cis* tetracoordinated complex (M_1), −2 235.082 88; *cis* tetracoordinated complex + noninteracting CO (M_1 + CO), −2 348.389 79.

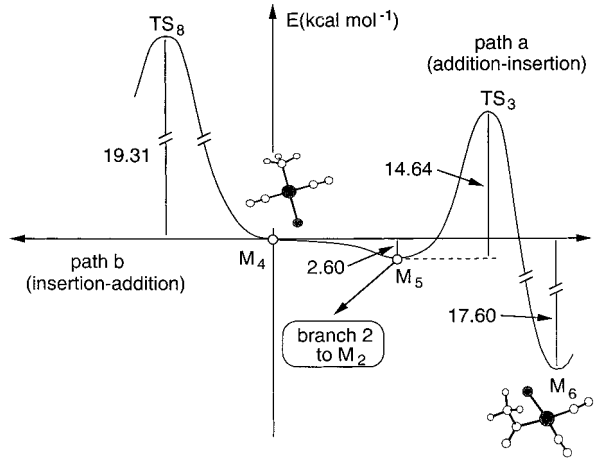

Figure 4. Schematic representation of the energy profiles for the two reaction paths a and b that originate from the *trans* four-coordinate complex M_4. The absolute energies (hartrees) are as follows: *trans* tetracoordinated complex (M_4), −2 235.085 98; *trans* tetracoordinated complex + noninteracting CO (M_4 + CO), −2 348.392 89.

(*trans* path). As found previously, M_4 also can bind an additional CO ligand, leading to the pentacoordinated complex M_5, which has a C_2 symmetry and all three CO ligands in equatorial positions. The final acyl product M_6 can be obtained through the transition state TS_3. This transition state is similar to TS_2 (located for the *cis* path) but has a stronger product-like character: the newly forming C_1-C_3 bond is shorter (1.826 Å) and the breaking C_2-C_3 bond is longer (2.159 Å). In M_6 the two remaining CO ligands are in *cis* positions and the newly formed acyl group lies in a plane orthogonal to the molecular plane.

We discuss now in a comparative way the energetics of the *cis* and *trans* reaction pathways (see the right sides of the diagrams of Figures 3 and 4). The formation of the pentacoordinated complex M_2 along the *cis* reaction path involves a very small barrier (1.86 kcal mol^{-1}). This barrier mainly originates from the rehybridization process that occurs on passing from the four-coordinated square-planar complex M_1 to the five-coordinated complex M_2; since the energy required to change the metal hybridization is gradually balanced by the energy obtained from the coordination of the additional CO ligand, the resulting barrier is very low. From the M_2 complex, which is degenerate to the system formed by the M_1 complex and a noninteracting CO molecule (M_1 + CO), we can obtain the final acyl product M_3 by overcoming a low barrier of 4.36 kcal mol^{-1}. The process is on the whole significantly exothermic, since the acyl complex is 20.09 kcal mol^{-1} lower in energy than reactants. This value is significantly higher than the exothermicity value of about 4 kcal mol^{-1} determined at the DFT level in ref 2m for the Cl(CO)-Ni···$COCH=CH_2$ system using both a local and a nonlocal approximation and a 6-311G** basis. Let us compare now this energy profile with that obtained for the *trans* isomer M_4 (right side of Figure 4), which is only 1.94 kcal mol^{-1} lower than the *cis* isomer M_1. The pentacoordinated complex M_5, which forms after binding an additional CO ligand, is 2.60 kcal mol^{-1} lower in energy than M_4 + CO. Even if a transition state exists leading from M_4 + CO to M_5, the surface in this region is so flat that we could not locate it using the available gradient method. This finding indicates that M_5 can form without almost any barrier from the four-coordinated *trans* species and an approaching CO molecule. However, even if no energy is required to form the pentacoordinated complex intermediate, a much higher insertion barrier (14.64 kcal mol^{-1}) must be overcome to obtain the final acyl product M_6, indicating that the channel involving the *trans* isomer is energetically less favorable than the channel starting from the *cis* isomer.

A transition state (TS_4) connecting the two pentacoordinated complexes M_2 and M_5 (pseudorotation or Berry mechanism) has also been located. This transition state is shown in Figure 2 and corresponds to the exchange of the chlorine atom from an equatorial (M_2) to an axial position (M_5). This transition state has a C_2 symmetry with the $Cl-Ni-C_2$ plane corresponding to the molecular symmetry plane. TS_4 is also characterized by a significant lengthening of the bonds between the metal atom and the two atoms involved in the pseudorotation: i.e., Cl and C_2, the two bonds Ni−Cl and Ni−C_2 being 2.403 and 1.937 Å, respectively (these bond lengths are 2.337 and 1.852 Å in M_2 and 2.286 and 1.846 Å in M_5). The reaction path connecting M_2 and M_5 is indicated as branch 1 in the diagram of Figure 3, and the corresponding energy profile is magnified on the bottom right of this figure. An activation barrier of 5.76 kcal mol^{-1} characterizes the transformation $M_2 \rightarrow TS_4 \rightarrow M_5$, while the reverse transformation $M_5 \rightarrow TS_4 \rightarrow M_2$ involves a barrier of 10.30 kcal mol^{-1}. These barriers

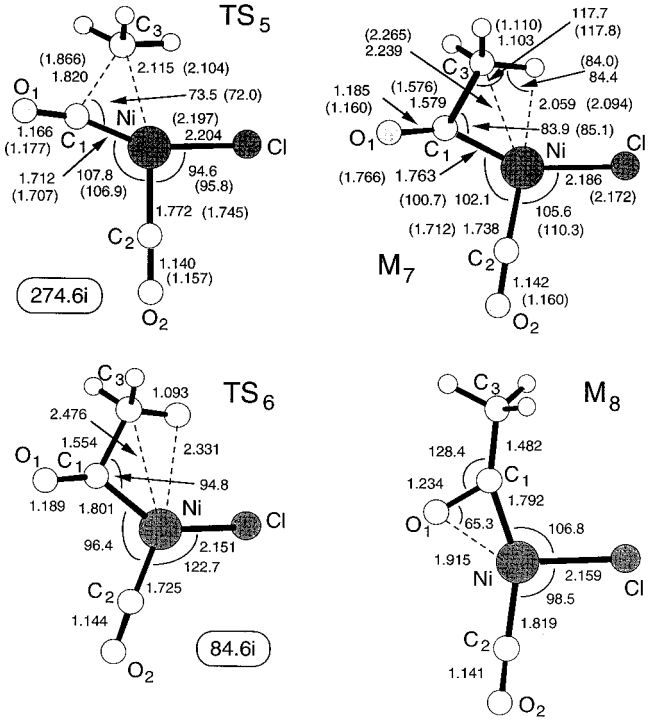

Figure 5. Schematic representation of the molecular structures found on path b for the *cis* four-coordinated complexes TS_5, M_7, TS_6, and M_8. Values were obtained with the B3LYP and BP86 (in parentheses) functionals (bond lengths are in angstroms and angles in degrees). The values of the imaginary frequency are reported for the transition structures.

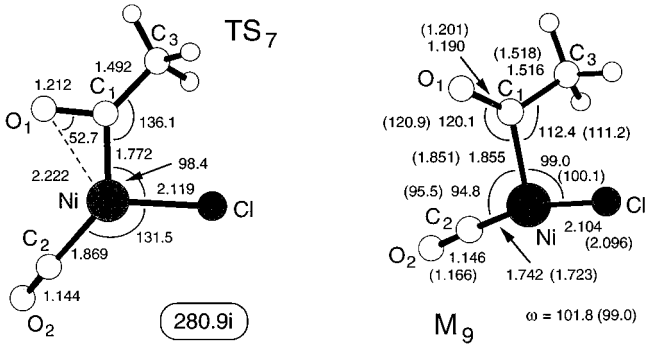

Figure 6. Schematic representation of the molecular structures found on path b for the *cis* four-coordinated complexes TS_7 and M_9. Values were obtained with the B3LYP and BP86 (in parentheses) functionals (bond lengths are in angstroms and angles in degrees). The values of the imaginary frequency are reported for the transition structures.

are not very high, as one might expect from the fact that the exchange from equatorial to axial positions of the trigonal bipyramid only requires changes in bond angles.

B. Path b (Insertion−Addition Mechanism). The formation of the tricoordinated acyl complex **4** (see Scheme 2) starting from the *cis* isomer along path b is a more complicated process than that associated with path a and involves two intermediates and the overcoming of three energy barriers. The molecular structures for the various critical points located along the reaction profile are schematically represented in Figures 5 and 6, while the corresponding energy values are reported on the left side of the diagram of Figure 3. The first transition state encountered on the reaction path is TS_5, which describes the migration of the methyl group from the metal to the carbon atom (C_1) of the carbonyl group. The breaking C_3-Ni bond is 2.115 Å, and the newly forming C_3-C_1 bond is 1.820 Å. These values are similar to those determined for the two transition states TS_2 and TS_3 located along path a for the *cis* and *trans* isomers, respectively. As found for TS_2 and TS_3, TS_5 also is a relatively early transition state, since the breaking $Ni-C_3$ bond is only 8% longer than in the tetracoordinated M_1 complex. TS_5 leads to the intermediate M_7, where the newly formed acyl group still interacts significantly with the metal atom. This interaction is a sort of C−H···Ni hydrogen bond, usually indicated as an α-agostic interaction, that involves the methyl hydrogens and is responsible of significant geometrical distortions: i.e., a lengthening of the C_1-C_3 and C_3-H bonds (1.579 and 1.103 Å, respectively) and an increase of the $H-C_3-C_1$ angle, which is 117.7° and thus quite larger than the usual tetrahedral angle. These stabilizing α-agostic interactions have been suggested to assist other catalyzed reactions, such as olefin insertion, during the polymerization processes.[12] Recently we have pointed out the existence of these agostic interactions (characterized by similar values of the C−H bonds) in a theoretical study on the Ziegler−Natta polymerization process.[13]

A second intermediate, M_8, forms through the transition state TS_6. In TS_6 the α-agostic interaction is weaker than in M_7 and the methyl group is moving away from the metal center: the C_3-Ni distance is now 2.476 Å and the $Ni-C_1-C_3$ angle is 94.8° (these two parameters are 2.239 Å and 83.9° in M_7, respectively). In M_8 the interaction between the methyl group and the nickel atom has been completely replaced by a strong interaction between the oxygen O_1 of the carbonyl group and the metal (the $Ni-O_1$ distance is only 1.915 Å). As a consequence the carbonyl bond (C_1-O_1) is significantly longer in M_8 (1.234 Å) than in M_7 (1.185 Å), while the C_1-C_3 bond is now much shorter (1.482 Å). A third transition state, TS_7, leads to the final three-coordinated acyl complex M_9 (**4** in Scheme 2), where the nickel−oxygen interaction has disappeared after a rotation around the $Ni-C_1$ bond (the dihedral angle ω between the two planes O_1-C_1-Ni and $C_1-Ni-Cl$ is now 101.8°). A computation of the intrinsic reaction pathway (IRC) starting from TS_6 and TS_7 in the reactant and product directions has shown how the various critical points are related.

The diagram of Figure 3 (left side) shows that the intermediate M_7 is 5.15 kcal mol^{-1} higher than the four-coordinated *cis* isomer and its formation requires the overcoming of a barrier of 6.83 kcal mol^{-1}. A very small barrier (only 0.56 kcal mol^{-1}) divides M_7 from the intermediate M_8, which is 3.95 kcal mol^{-1} higher than M_1. This low barrier is mainly due to the loss of the stabilizing α-agostic interaction between the methyl hydrogen and the nickel atom. The final step, i.e., the formation of the three-coordinated acyl complex M_9 from M_8, is characterized by an activation energy of 8.47 kcal

(12) (a) Kawamura-Kuribayashi, H.; Koga, N.; Morokuma, K. *J. Am. Chem. Soc.* **1992**, *114*, 2359. (b) Weiss, H.; Ehrig, M.; Ahlrichs, R. *J. Am. Chem. Soc.* **1994**, *116*, 4919.

(13) Bernardi, F.; Bottoni, A.; Miscione, G. P. *Organometallics* **1998**, *17*, 16.

mol^{-1} (transition state TS_7) that is mainly determined by the loss of the stabilizing interaction between the carbonyl oxygen O_1 and the metal atom. The whole process is only slightly exothermic, since M_9 is 2.61 kcal mol^{-1} lower in energy than the starting *cis* complex.

The insertion transition state TS_8, similar to TS_5, has been also located for the *trans* isomer (this structure is schematically represented in Figure 7). However, as found for path a, for path b also the channel that originates from the *trans* isomer is energetically much less favorable than that associated with the *cis* isomer, since the insertion energy barrier computed in the former case (19.31 kcal mol^{-1} as reported on the left side of the diagram of Figure 4) is much higher than all three barriers found in the latter.

C. Comparison between Path a and Path b for the *cis* Isomer. In the discussion of the previous sections we have demonstrated that path a (addition−insertion path) leads directly to a four-coordinated acyl complex (acyl product M_3) through transition state TS_2, while path b (insertion−addition path) leads first to the formation of a three-coordinated acyl complex (M_9) that is highly unsaturated; this complex can bind easily an additional CO molecule to give the final product M_3, as schematically indicated in the diagram of Figure 3 (no energy barrier has been found for this process). This diagram clearly indicates that, for the model system considered here, path a is energetically more convenient than path b to reach the tetracoordinated acyl complex M_3 (the rate-determining step in the former case has a barrier of 4.36 kcal mol^{-1}, while in the latter case two energy barriers of 6.83 and 8.47 kcal mol^{-1}, respectively, are involved). However, a further investigation of the potential surface has shown the existence of an additional reaction channel starting from the intermediate M_8 on path b (branch 2 in Figure 3). M_8 can bind easily a new CO ligand to give the tetracoordinated acyl complex M_6. The energy profile for branch 2 is magnified in the diagram of Figure 3 (bottom left); this channel involves the formation of a preliminary intermediate (M_{10} represented in Figure 7) that corresponds to a loosely bound complex between the new CO ligand and M_8 (the carbon atom of the carbonyl group only weakly interacts with the metal atom, the nickel−carbon distance being 2.886 Å). This intermediate is 2.40 kcal mol^{-1} lower in energy than the asymptotic limit (M_8 + CO). From M_{10} this path leads to the tetracoordinated acyl complex M_6, which is 23.49 kcal mol^{-1} lower than M_8 + CO. This process requires the overcoming of a negligible barrier of 0.11 kcal mol^{-1} (transition state TS_9 in Figure 7). Even if the physical meaning of the shallow minimum corresponding to M_{10} and that of the transition state TS_9 are questionable (this type of depression on the potential surface could just be a mere computational shortcoming due to a basis set superposition error), the results undoubtedly indicate that, in the presence of additional CO molecules, from M_8 it is possible to obtain easily the tetracoordinated acyl complex M_6. Thus, branch 2 represents an easy way to obtain the final acyl product and to avoid the need of overcoming a barrier of 8.47 kcal mol^{-1}. It is interesting to point out that branch 1 also can lead to the product acyl complex M_6 through the Berry pseudorotation. However, this path is energetically much less convenient since, as pointed out in the previous section, it requires the overcoming of an insertion barrier of 14.64 kcal mol^{-1} (transition state TS_3).

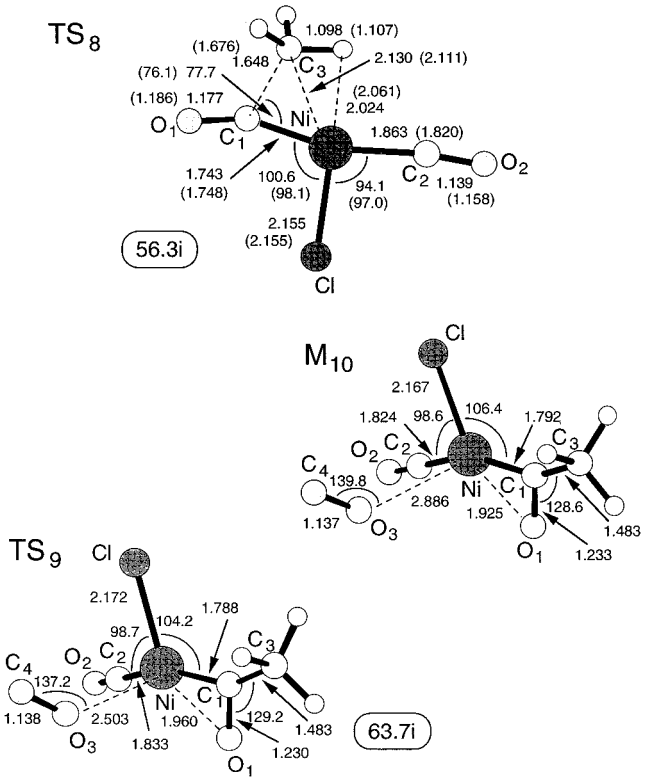

Figure 7. Schematic representation of the insertion transition state TS_8 found on path b for the *trans* four-coordinated complex and of the two critical points M_{10} and TS_9 located along branch 2. Values were obtained with the B3LYP and BP86 (in parentheses) functionals (bond lengths are in angstroms and angles in degrees). The values of the imaginary frequency are reported for the transition structures.

All these computational results suggest that in the real experimental system the two reaction channels starting from the *cis* isomer (path a and path b + branch 2) can easily compete, depending on the experimental conditions that are used: the temperature, the type of solvent, and the excess of CO used to carry out the reaction. For instance, the equilibrium between the two complexes M_1 and M_2 (M_1 + CO = M_2) can be significantly shifted to the right in the presence of an excess of the CO ligand, favoring path **a**.

The nature of the potential surface with two competitive reaction channels, both leading to carbonylation products, confirm the mechanistic scheme suggested by Garrou and Heck.[1e] For a similar reacting system, i.e., M(R)(Cl)$(PR'_3)_2$ + CO (M = Pt, Pd, Ni), they found that, in the presence of an excess of phosphine ligands, carbonyl insertion takes place directly on a five-coordinated complex, while without additional phosphine the reaction involves a four-coordinated intermediate.

D. Diabatic Model. The trend of the insertion barriers between the two five-coordinated complexes M_2 and M_5 or between the *cis* and *trans* four-coordinated isomers M_1 and M_4 can be rationalized by means of a simple diabatic model based upon spin recoupling in VB

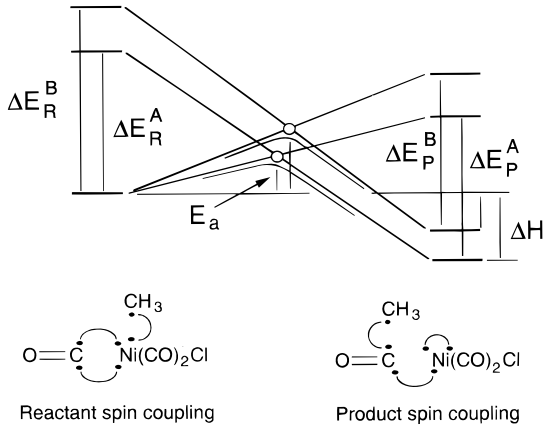

Figure 8. Diabatic diagram for the insertion reaction involving the two five-coordinate complexes M_2 and M_5.

theory.[14] Within this model the reaction energy profile is decomposed into two component curves: a *reactant diabatic* and a *product diabatic*. These two curves describe the energy behavior along the reaction coordinate of the electronic configurations associated with the reactant spin coupling (*reactant bonding situation*) and the product spin coupling (*product bonding situation*), respectively. The reactant diabatic, on passing from reactants to products, is repulsive, while the product diabatic is attractive. The crossing between the two diabatics determines the position of the transition state and the magnitude of the activation energy.

We use this model to discuss in detail the insertion process for the two pentacoordinated complexes M_2 and M_5. Similar arguments can be used to compare the *cis* four-coordinated isomer M_1 and the *trans* isomer M_4. Figure 8 shows the qualitative behavior of the reactant and product diabatics for the two complexes M_2 and M_5. We assume that the Ni−C(carbonyl) bond (Ni−C_1) can be represented to a good approximation by a double bond and the Ni−C(methyl) bond (Ni−C_3) by a single σ bond. Thus, the reactant diabatic corresponds to a situation where the two electrons of the σ Ni−C(methyl) bond are coupled to a singlet and the same happens for the four (σ and π) electrons of the Ni−C(carbonyl) bond (reactant coupling). In the product diabatic the π electron of the CO group is singlet spin-coupled with the methyl electron to form the new C(carbonyl)−C(methyl) bond (C_1−C_3) in the acyl product, while the remaining two electrons on the nickel atom are coupled to a singlet in a lone pair (product coupling). The reactant and product spin couplings are schematically represented at the bottom of Figure 8.

In these types of diagrams three factors concur to determine the position of the crossing and the size of the barrier (see Figure 8): (i) ΔH, i.e., the energy difference between the product diabatic at the product geometry and the reactant diabatic at the reactant geometry, which corresponds approximately to the reaction enthalpy; (ii) ΔE_R (left side of the diagram), i.e., the energy difference between the reactant and product diabatic at the reactant geometry; (iii) ΔE_P (right side of the diagram), i.e., the energy difference between the reactant and product diabatic at the product geometry.

ΔH can be estimated on the basis of the computed quantum-mechanical energy values of reactants and products. From Figures 3 and 4 it is evident that the reaction is more exothermic for M_2 ($\Delta H = -20.09$ kcal mol^{-1}) than for M_5 ($\Delta H = -15.00$ kcal mol^{-1}). ΔE_R is approximately determined by the algebraic sum of three contributions: (a) the energy required for decoupling the electron pair associated with the σ Ni−C(methyl) bond (destabilizing positive term); (b) the energy needed for decoupling the two electrons of the π component of the Ni−C(carbonyl) bond (destabilizing positive term); (c) the energy obtained after coupling the two electrons of the metal lone-pair (stabilizing negative term). Furthermore, we can reasonably assume that the coupling of the remaining two electrons is energetically negligible since, at the reactant geometry, these electrons are too far away (one electron on the C(methyl) atom and the other on the C(carbonyl) atom). The three contributions a−c can be evaluated to a good approximation from the energies of the corresponding bonds. The energy of the Ni−C(methyl) bond can be expected to be lower in the M_2 complex than in the M_5 complex. This can be explained on the basis of a *trans* influence,[15] which is stronger in the former case than in the latter. This *trans* influence is due to the carbonyl group, which is axial in the M_2 complex and makes the Ni−C(methyl) bond (*trans* to the CO group) weaker in M_2 with respect to M_5. We have roughly evaluated the strength of this bond in both M_2 and M_5,[16] and we have found value of 45.5 and 47.6 kcal mol^{-1}, respectively, in agrement with the *trans* influence hypothesis. The π component of the Ni−C(carbonyl) bond can be reasonably assumed to be roughly constant in M_2 and M_5, since no *trans* influence can be envisaged for the CO group involved in the insertion: this group is equatorial in both complexes and has no *trans* ligand. A similar assumption can be made for the metal lone pair. Thus, the key factor which determines the variation of ΔE_R on going from M_2 ($\Delta E_R{}^A$) to M_5 ($\Delta E_R{}^B$) is the variation of the Ni−C(methyl) bond energy and consequently $\Delta E_R{}^A < \Delta E_R{}^B$.

In a similar way we obtain an estimate of ΔE_P in the two acyl products M_3 (obtained from M_2) and M_6 (obtained from M_5). The contributions that determine the magnitude of ΔE_P are (d) the energy required to break the C(carbonyl)−C(methyl) bond, which cannot change significantly on passing from M_3 to M_6, (e) the energy needed for decoupling the two electrons of the metal lone pair, which is also approximately constant in the two complexes, and (f) the energy obtained from the coupling of the two electrons on the C(carbonyl) and nickel atoms. This last contribution should be slightly more stabilizing in the acyl product M_3 than in the product M_6 since the Ni−C(carbonyl) bond length is significantly shorter in the former case (1.915 Å) than in the latter (1.943 Å). This contribution should make $\Delta E_P{}^A$($M_2 \rightarrow M_3$ process) smaller than $\Delta E_P{}^B$($M_5 \rightarrow M_6$ process).

(14) (a) Pross, A.; Schaik, S. S. *Acc. Chem. Res.* **1983**, *16*, 363. (b) Bernardi, F.; Olivucci, M.; McDouall, J. J. W.; Robb, M. A. *J. Chem. Phys.* **1988**, *89*, 6365.

(15) (a) Quagliano, J. V.; Shubert, L. *Chem. Rev.* **1952**, *50*, 201. (b) Chatt, J.; Duncanson, L. A.; Venanzi, L. M. *J. Chem. Soc.* **1955**, 4456.

(16) To evaluate the strength of the Ni−C_3 bond in the two pentacoordinated complexes M_2 and M_5, we have carried out DFT(B3LYP)/6-31G* computations on the two radical fragments $H_3C^\bullet$ and $^\bullet Ni(CO)_3Cl$ and taken the energy difference between the composite systems and the two noninteracting fragments. A similar approach has been used for the two tetracoordinated complexes M_1 and M_4.

In conclusion, all three factors (ΔH, ΔE_R, and ΔE_P) have the effect of making the insertion barrier associated with the M_2 complex lower than that for the M_5 complex, as found in our computations. The trend of these factors can also help to determine the relative position of the two transition states (TS_2 and TS_3) with respect to reactants and products. From the diagram of Figure 8 it is evident that the decrease of ΔH and ΔE_R on going from M_2 to M_5 makes TS_2 more reactant-like than TS_3. This foresight on the nature of the insertion transition state is in agreement with the computational results reported in Figures 1 and 2: in TS_2 the newly forming C_1-C_3 bond (1.986 Å) is significantly longer than in TS_3 (1.826 Å), while the breaking $Ni-C_3$ bond is shorter (2.112 and 2.159 Å, respectively).

Conclusion

In this paper we have used a DFT approach to carry out a theoretical study of the carbonylation process on the model system formed by the methylnickel complex $CH_3Ni(CO)_2Cl$, which reacts with an additional CO molecule. We have found that two different reaction channels, both originating from the *cis* four-coordinated isomer, can lead to the carbonylation products (acyl complexes): one reaction path (path a) involves a five-coordinate complex where the carbonyl insertion takes place; the other reaction path (path b) is characterized by the formation of four-coordinate complexes. If we consider the formation of one of the two possible tetracoordinated acyl products, i.e., M_3 (where the two CO ligands are in *trans* positions), path a is energetically favored with respect to path b (an energy barrier of 4.36 kcal mol^{-1} must be overcome along path a, while two barriers of 6.83 and 8.47 kcal mol^{-1} are involved along path b). However, on path b a side channel starting from the intermediate M_8 (branch 2 in Figure 3) represents an alternative and easy way for obtaining the second acyl product M_6, where the two CO ligands are in *cis* positions. Thus, along path b the second acyl product M_6 can be obtained by overcoming only the first barrier of 6.83 kcal mol^{-1}.

These results can be interpreted as follows: even if for our model system path a is energetically slightly more convenient than path b + branch 2, for the real system the two reaction paths can be highly competitive and their relative importance can be determined by the experimental conditions. Our computational results are in agreement with the experimental evidence obtained by Garrou and Heck[1e] for a similar system, i.e., $M(R)(Cl)(PR'_3)_2 + CO$ (M = Pt, Pd, Ni), but they are slightly different from the computational finding of De Angelis et al.[2m] These authors studied the Reppe carbonylation of alkenes on the model system formed by the $Cl(CO)_2NiCH{=}CH_2$ complex and found that the migrative insertion of CO into the metal−vinyl bond takes place only on a *cis* four-coordinated complex.

Appendix. Comparison between B3LYP and BP86 Computations

To check the reliability of the results obtained with the hybrid B3LYP functional, we have recomputed some significant critical points for both paths a and b with the pure BP86 functional and the same basis set used in the B3LYP computations. We have chosen this functional since we have recently demonstrated that it provides (like B3LYP) reliable results (when compared to theoretical CASPT2 results and experimental data) for nickel complexes with unsaturated olefin ligands.[17] The values of the geometrical parameters obtained at the BP86 level are reported in parentheses in Figures 1, 2, and 5−7, while the corresponding energy values are collected in Table 1.

Table 1. Relative Energies (E, kcal mol^{-1})[a] of the Various Critical Points Associated with Path a and Path b for the *cis* and *trans* Isomers Computed at the BP86 Computational Level

cis isomer		*trans* isomer	
	Path a		
$M_1 + CO$	0.00	$M_4 + CO$	0.00
M_2	−8.04	M_5	−13.72
TS_2	−3.92	TS_3	−1.98
M_3	−23.88	M_6	−28.60
	Path b		
M_1	0.00	M_4	0.00
TS_5	5.14	TS_8	14.17
M_7	2.53		
M_9	−4.47		

[a] The absolute energies (hartrees) are as follows: *cis* tetracoordinated complex + noninteracting CO (M_1 + CO), −2 348.659 49; *trans* tetracoordinated complex + noninteracting CO (M_4 + CO), −2 348.655 61; *cis* tetracoordinated complex (M_1), −2 235.354 30; *trans* tetracoordinated complex (M_4), −2 235.350 42.

For path a all the critical points (except TS_1) have been recomputed at the BP86 level. In all cases the geometrical parameters obtained with the pure BP86 functional are very similar to those computed at the B3LYP level. Only small variations in the bond lengths and bond angles are observed in both *cis* and *trans* square-planar four-coordinated complexes M_1 and M_4 on passing from the hybrid B3LYP to the pure BP86 functional. For instance, the two $Ni-C_1$ and $Ni-C_2$ bonds become slightly shorter in both M_1 (from 2.202 to 2.201 Å and from 1.738 to 1.719 Å) and M_4 (from 1.808 to 1.779 Å and from 1.795 to 1.770 Å), while the $Ni-C_3$ bond and the two C_1-O_1 and C_2-O_2 bonds become slightly longer (the $Ni-C_3$ bond changes from 1.963 to 1.977 Å in M_1 and from 1.950 to 1.958 Å in M_4). Similar trends are observed in the two pentacoordinated complexes M_2 and M_5. The two insertion transition states TS_2 and TS_3 are slightly more reactant-like at the BP86 level: for instance, in TS_2 the $Ni-C_3$ bond becomes 2.108 Å (2.112 Å at the B3LYP level), while the newly forming C_3-C_1 bond is 2.056 Å and the C_3-Ni-C_1 angle is 64.1° (1.986 Å and 61.4° are the corresponding B3LYP values). Also, for the two final four-coordinated acyl complexes M_3 and M_6 the BP86 functional provides a description that is very similar to that obtained at the B3LYP level. Inspection of Table 1 shows that, even if at the BP86 level the formation of the two five-coordinated complexes M_2 and M_5 becomes an exothermic process (at the B3LYP level the five- and four-coordinated complexes are almost degenerate in energy), the two insertion barriers leading to M_3 and M_6 do not change significantly, being 4.12 and 11.74 kcal mol^{-1}, respectively. Thus, also at the BP86 level the insertion process involving the *cis* isomer is favored with

(17) Bernardi, F.; Bottoni, A.; Calcinari, M.; Robb, M. A.; Rossi, I. *J. Phys. Chem. A* **1997**, *101*, 6310.

respect to the corresponding process associated with the *trans* isomer.

For path b we have recomputed at the BP86 level the insertion transition state TS_5 associated with the *cis* isomer, the corresponding intermediate M_7, the final three-coordinated acyl product M_9, and the insertion transition state TS_8 associated with the *trans* isomer. As found for the five-coordinated complex, both TS_5 and TS_8 become slightly more reactant-like at the BP86 level: for TS_5 the C_3-C_1 bond and the C_3-Ni bond change from 1.820 to 1.866 Å and from 2.115 to 2.104 Å, respectively. The M_7 intermediate is again characterized by an α-agostic interaction involving one methyl hydrogen atom and the nickel atom (the C_3-H distance is 1.111 Å) and by a nonnegligible interaction between the methyl carbon C_3 and the metal atom. These interactions are responsible for geometrical distortions similar to those observed at the B3LYP level, such as the anomalous value of the $H-C_3-C_1$ angle (117.8°). Table 1 shows that the two insertion barriers associated with TS_5 and TS_8 are 5.14 and 14.17 kcal mol^{-1}, respectively which must be compared to the B3LYP values of 6.83 and 19.31 kcal mol^{-1}.

All these results indicate that the pure BP86 functional provides information that is very similar to that obtained with the hybrid B3LYP functional: (i) the insertion process involving the *cis* isomer is favored with respect to the corresponding process associated with the *trans* isomer for both path a and path b; (ii) the two channels (a and b) associated with the *cis* isomer require the overcoming of similar activation energies, and both can be important to obtain the final acyl products.

Acknowledgment. We thank the CNR, MURST (Progetto Nazionale "Stereoselezione in Sintesi Organica, Metodologie ed Applicazioni"), and Bologna University (Funds for Selected Research Topics) for financial support of this research.

OM990808W